Photon Upconverting Nanoparticles for Luminescent Sensing of Temperature

Andreas Sedlmeier, Daniela E. Achatz, Lorenz H. Fischer, Hans H. Gorris*, Otto S. Wolfbeis*

Received (in XXX, XXX) Xth XXXXXXXXX 20XX, Accepted Xth XXXXXXXXX 20XX
DOI: 10.1039/b000000x

Photon upconverting nanoparticles convert near-infrared into visible light (anti-Stokes emission), which strongly reduces the background of autofluorescence and light scattering in biological materials. Hexagonal $NaYF_4$ nanocrystals doped with Yb^{3+} as the sensitizer and Er^{3+}/Ho^{3+}/Tm^{3+} as the activator display at least two emission lines that respond differentially to temperature changes. The ratio of the main emission line intensities enables a self-referenced optical readout of the temperature in the physiologically relevant range from 20 to 45°C. Upconverting nanoparticles of the type $NaYF_4$:Yb,Er covered by an inactive shell of $NaYF_4$ are bright and allow for resolving temperature differences of less than 0.5°C in the physiological range. The optical readout of this nanoparticle-based thermometer offers many options for imaging the two-dimensional distribution of temperature.

1. Introduction

Temperature (T) is by far the parameter most often measured in science and technology. Examples can be found in physical, chemical and biological applications. Temperature changes in cell cultures as well as the efficiency of cooling systems in chemical reactors or bioreactors are identifiable by means of temperature monitoring.[1] The knowledge of the exact temperature is generally important for the optimization of photothermal cancer therapy[2] and for the investigation of cellular processes like enzyme reactions or metabolism[3]. Aside from conventional (scale) thermometry, sensors based on the measurement of electrical resistance, thermistors, or thermocouples are in widespread use.[1,4] They all require the sample and the sensor to be in direct contact. Non-contact techniques are of the optical type and rely, for example, on the T dependence of the infrared (IR) emission of an object. Infrared (IR) thermometry is widely used, enables imaging, but lacks spatial resolution. Also, the high absorption of infrared radiation by glass materials and water vapor limits the applicability of this measurement type. Alternatively, the effect of T on the luminescence may be exploited.[1] Optical techniques have the specific advantage of being applicable in even strong magnetic fields and in corrosive environments.[5]

Parameters of fluorescence that, more or less, depend on T include intensity, decay time (lifetime) and the shapes of excitation and emission spectra.[1,6,7] Lifetime-based methods have favorable aspects like self-referencing, ease of calibration and suppression of background via gating techniques.[6,8,9] Methods based on ratioing the intensities of two emissions are more simple but require the luminescent material to display multiple emissions whose response to T has to be different. They are intrinsically referenced and independent of excitation power[10]. In a typical approach, the fluorescence intensities of the two emission bands are determined under single-wavelength excitation, and their ratio is related to T.[5,11] The ratio of intensities has to depend, of course, solely on temperature in order to be applicable to thermometry.[12]

There is a substantial interest in nanosized optical probes for T because they will enable T to be sensed with nm resolution. Various kinds of respective nanoparticles have been reported.[5,7,13,14] Materials in nanoscale dimensions also enable bio- and nanotechnological applications because larger particles, e.g. on the order of micrometers, result in a limited spatial resolution and accuracy, and certainly cannot be used in cellular studies because of their size.[13] Nanoparticles based on europium chelates[5,14], terbium complexes[7,9] or a dye linked to semiconducting polymers[15] are suitable options. However, these materials show certain drawbacks like excitation with ultraviolet light which are limiting their use in biological applications.

Upconverting luminescent nanoparticles (UCLNPs) represent a rather new nanomaterial that has attractive features: UCLNPs emit two or more narrow emission peaks[16] in the visible spectral range upon photoexcitation in the near IR (800 – 1000 nm)[17,18] (anti-Stokes emission). NIR excitation results in good penetration of tissue and in low background fluorescence of biological specimen.[17,19] Hexagonal $NaYF_4$ doped with erbium (the activator) and ytterbium (the sensitizer) represents the material with the highest upconversion efficiency reported so far.[18,20,21] Additionally, such UCLNPs exhibit low cytotoxicity[19,22]. Both features are essential for intracellular studies.

The luminescence of UCLNPs is strongly temperature dependent and the multiple emission lines respond differently to temperature changes. For example, the intensity of the $^4S_{3/2} \rightarrow {}^4I_{15/2}$ transition (green emission at 523 nm) is higher than that of the $^2H_{11/2} \rightarrow {}^4I_{15/2}$ transition (green emission at 545 nm) at low temperatures in Er^{3+} doped UCLNPs but this is inverted at higher T.[16,23] The sensitivity to T also depends on the synthesis and size of the upconversion material. An annealing step at high temperatures during the co-precipitation synthesis transfers the cubic into the hexagonal crystal phase which is brighter and than the cubic modification and more sensitive to T. This annealing temperature affects the energy gap between the two excited levels.[23] In general, T has a larger effect on nanosized crystals than on the respective bulk material, probably because surface defects become increasingly important when the particle diameter decreases.[16,24] Surface quenching effects also reduce the brightness of UCLNPs as well as the quantum yield (QY).[25,26] These effects, however, can be reduced by a core-shell structure. A thin layer of undoped host material grown on the surface of UCLNPs strongly increases their emission intensity[25], in some

cases by a factor of ~ 7. [27]

The use of UCLNPs for thermometry was recently reviewed[13]. Dong et al. achieved temperature resolution of 0.3°C by using Al_2O_3 as the host material and Er^{3+} and Yb^{3+} as dopants.[28,29] Nanoparticles consisting of Gd_2O_3 doped with Er^{3+} and Yb^{3+} were employed by Singh et al.[16]. Alencar et al.[24] investigated Er^{3+} doped $BaTiO_3$ nanocrystals regarding their temperature dependency of the upconversion emission.

Also, host materials doped additionally with transition metals were studied. For example, Dong et al. investigated $Yb_3Al_5O_{12}$ nanoparticles doped with Er^{3+}/Tm^{3+}, Yb^{3+} and molybdenum.[30] Vetrone et al. measured the temperature distribution in HeLa cells by using UCLNPs of the type $NaYF_4$:Yb^{3+},Er^{3+} in the cubic modification.[31]

Here, we systematically investigate the ratiometric temperature response of UCLNPs with a hexagonal $NaYF_4$ host lattice, which is the most efficient upconversion material known to date.[20,21] Dopant combinations of Er^{3+}, Ho^{3+} or Tm^{3+} and Yb^{3+} as the sensitizer are analyzed regarding their temperature resolution in the physiological range. These nanoparticles were prepared as both core-only and core-shell structures.

2. Experimental section

2.1. Instrumentation

The instrumental setup is shown in **Figure 1**. It consists of a Lauda MGW RC6 thermostat (www.lauda.de), an adjustable 980-nm continuous wave laser diode with a maximal power of 5 W (from Roithner Lasertechnik; www.roithner.at), a Pt-100 resistance thermometer (model GMH3710; from Greisinger; www.greisinger.de), optical fiber waveguides, and cuvettes (1 x 1 x 3 cm^3) contained in a fluorometer (Cary Eclipse; from Varian; www.varian.com).

The thermostat was linked to the cuvette holder containing dispersions of the nanoparticles by two silicone tubes that were thermally isolated. Water of defined temperature was pumped through the tubes to pass a cavity in the cuvette holder. Light of a 980-nm laser diode (power applied: 3 – 4 W) was guided to the sample in the cuvette via an optical fiber waveguide. The cuvette was covered with a Teflon lid. The resistance thermometer was placed in the cuvette, and its wiring was inserted through the Teflon cover.

Transmission Electron Microscopy (TEM) was performed using a 120-kV Leo 912AB (www.zeiss.com) equipped with a CCD camera (www.proscan.com), at the Department of Pathology of the Regensburg University Hospital.

2.2. Syntheses of UCLNPs

All particles employed in this study had a molar percentage (referred to the total amount of rare earth ions) of 20 % for Yb^{3+}, 2 % for Er^{3+} and of 0.5 % for X = Ho^{3+} and Tm^{3+}, respectively. All these particles were obtained by the following syntheses.

Particles of the type UCLNP-I and UCLNP-IV were prepared according to the co-precipitation method of Guo et al.[32]: YCl_3, $YbCl_3$ and XCl_3 (X = Er, Ho, Tm) were dissolved in double distilled water (pH = 2) to obtain stock solutions with a concentration of 0.2 M. Defined volumes of these solutions were mixed with a 0.2 M Titriplex III stock solution depending on the desired doping grade. Furthermore, a solution of 2.1 g NaF (0.05 mol) in 60 mL double distilled water was prepared. The EDTA-salt solution was injected quickly into this solution and the resulting mixture was stirred for one hour at room temperature. The obtained precipitates were centrifuged and washed three times with double distilled water and once with ethanol. The washing steps included sonication to redisperse the nanoparticles. The precipitates were then dried at 75 °C for 90 minutes. The resulting white powder was split up into 100 mg aliquots (batches) by transferring them into round-bottom flasks (10 mL). Subsequently, the particles were sintered under an argon atmosphere at a temperature of 400 °C for 5 hours. Afterwards the flasks were left to cool to room temperature. The 100 mg aliquots were not combined, treated as different batches and stored in snap cap bottles.

The thermal decomposition method by Zhang[33] results in purely hexagonal particles of the type UCLNP-II, UCLNP-V and UCLNP-VI. The synthesis was carried out as follows: The lanthanide salts YCl_3, $YbCl_3$ and XCl_3 (X = Er, Ho, Tm) were added to a mixture of 3 mL oleic acid (OA) and 17 mL octadecene (ODE) in a 50 mL flask. The amounts of these salts were adjusted to the desired doping grade of the UCLNPs. The solution was heated to 160 °C in order to obtain a homogenous mixture. After cooling to room temperature a solution of NaOH (0.01g) and NH_4F (0.148 g) in 10 mL methanol was added slowly and the mixture was stirred for 30 minutes at room temperature. The methanol was evaporated at 70 °C. The solution was heated to 300 °C under an argon atmosphere for an hour. The mixture was cooled to room temperature. Ethanol was added to precipitate the hydrophobic oleic acid coated particles. The nanoparticles were washed three times with ethanol/water (1:1 v/v). Ligand exchange[34] was employed to replace the hydrophobic oleic acid on their surface by citric acid to obtain particles that can be dispersed in water. This process included the following steps: The nanoparticles coated with oleic acid (120 mg) were dispersed in a (1:1) mixture of 1,2-dichlorobenzene and N,N'-dimethylformamide (DMF) (total volume: 15 mL). After the addition of 0.1 g citric acid (CA) the mixture was stirred at 100 °C for approximately 24 hours. The hydrophilic particles were precipitated by adding ethyl ether (ca. 40 mL). The particles were washed by redispersion in acetone and centrifugation. The supernatant was removed and the remaining solvent was allowed to evaporate.

The core-shell type of nanoparticles (UCLNP-III) contain a hexagonal β-$NaYF_4$ core doped with Yb^{3+}/Er^{3+} and an inactive β-$NaYF_4$ shell and were synthesized according to Guo et al.[35] with certain modifications: $YCl_3 \cdot 6\ H_2O$ (0.5 mmol, 0.1517 g) were dissolved in 3 mL oleic acid and 7.5 mL octadecene at 150 °C. A dispersion of 94 mg nanoparticles of the type $NaYF_4$: Yb, Er in 5 mL hexane was added dropwise. The hexane solution was evaporated by heating to 80 °C under an argon flow. Ammonium fluoride (2 mmol, 0.0742 g) and sodium hydroxide (1.25 mmol, 0.05 g), dissolved in 10 mL methanol, were added dropwise to the cooled oleic acid/octadecence solution. Afterwards, the mixture was stirred slowly for 30 minutes at room temperature. The solvent methanol was evaporated by heating to 80 °C under an argon flow. The remaining mixture was heated to 260 °C

under an argon flow and then stirred for 1 hour at 260 °C without argon. The solution was cooled to room temperature. The particles were precipitated by adding 15 mL acetone and washed (2x with ethanol, 1x with acetone).

2.3. Sample preparation and measurement

Particles were dispersed in doubly distilled water (10 mL) in concentrations of ~1.25 mg mL^{-1} by sonication for 15 min. The solutions were filtered through a disc filter (PTFE; 5 µm pore size) to remove agglomerates and sonicated for another 3 min prior to each measurement. The dispersions were stirred slowly during the measurements to prevent sedimentation and to obtain a uniform heat distribution.

Each calibration consisted of five measurements in covered cuvettes. Spectra of samples were acquired in cuvettes which were heated from 20 to 60 °C in steps of 5 °C under stirring. The emission spectra were recorded at each temperature. The sample was cooled to 20 °C and a new cycle was started. Five cycles were run in each case.

3. Results

3.1. Characteristics of upconverting luminescent nanoparticles (UCLNP) employed

The different particle types used in this study and their figures of merit are summarized in **Table 1**. The preparation, size and surface ligands exert a strong effect on the characteristics of the particles. Accordingly, the dispersibility depends on the surface, the upconversion efficiency on the $NaYF_4$ modification and the sedimentation rate on the size and the surface. The ligand citric acid together with the lower size in case of UCLNP-II/V/VI improves the dispersibility and reduces the tendency towards sedimentation compared to the particles of the type UCLNP-I/IV with ETDA ligands. Also the upconversion efficiency and, hence, the emission intensity is higher because of the presence of purely hexagonal $NaYF_4$ instead of a mixture of a hexagonal (β-$NaYF_4$) and a cubic (α-$NaYF_4$) phase. An additional layer of β-$NaYF_4$, i.e. an inactive shell, increases the emission intensity ("brightness") by reducing surface quenching effects.[25]

Figure 2 shows the TEM images of the three erbium-doped particle types UCLNP-I to UCLNP-III. The images of UCLNP-IV to UCLNP-VI are not depicted because they are very similar as the respective erbium-doped particles (UCLNP-I → UCLNP-IV, UCLNP-II → UCLNP-V/VI). All three images show that the different types of particles do not aggregate. The core-shell structure of the UCLNP-III is not visible in the TEM image because the core and the shell are composed of the same host material. While the dopant ions of the core do not change the TEM contrast noticeably, the core-shell structure is evident from the increase of the particle diameter. The UCLNP-II consist only of doped material and have an average diameter of 28 nm (**Figure 2b**). These nanoparticles serve as a precursor for the generation of the core-shell particles UCLNP-III that have a larger average diameter of 32 nm (**Figure 2c**).

The materials with the highest upconversion efficiency reported so far consist of $NaYF_4$ doped with Yb^{3+} (the sensitizer) and Er^{3+} (the activator).[20,19] This results in the highest brightness which is critical in case of intracellular studies. **Figure 3** shows the emission spectra of UCLNP-I dispersed in water. Main emission peaks can be found at 521, 541 and 656 nm. Particles of type UCLNP-II and UCLNP-III display virtually identical spectra and similar temperature dependence. The transitions for the three main bands can be assigned to $^4F_{9/2} \rightarrow {}^4I_{15/2}$ (peak A), $^4S_{3/2} \rightarrow {}^4I_{15/2}$ (peak B) and $^2H_{11/2} \rightarrow {}^4I_{15/2}$ (peak C) transitions.[29] Additionally, two other activator species, i.e. holmium (Ho^{3+}) and thulium (Tm^{3+}), were investigated regarding their applicability for temperature measurements. The spectra of these dopants in a water dispersion are shown in **Figure 4**. The bands employed for ratiometric evaluation are at 541 nm (transition: $^5S_2 \rightarrow {}^5I_8$) and at 656 nm (transition: $^5F_5 \rightarrow {}^5I_8$) for holmium[36] and at 475 nm (transition: $^1G_4 \rightarrow {}^3H_6$) and at 695 nm (transition: $^3F_3 \rightarrow {}^3H_6$) for thulium.[37,38]

3.2. Temperature dependencies of the luminescence

The temperature range (20°C – 60°C) and solvent (water) were chosen because of the intended application of these particles in an aqueous biological environment. The temperature dependency of the transitions of erbium is shown in **Figure 5**. There is virtually no change in the signal intensity of the peak at 523 nm for all three kinds of particles. Both the 541 nm and the 656 nm emissions of the UCLNP-I particles noticeably decrease with increasing temperature (**Figure 5a**). Particles coated with citric acid ligands, i.e. UCLNP-II and UCLNP-III, show a strong decrease in intensity at 541 nm but less so at 656 nm (**Figure 5b-5c**). The greatest dependence on T of all emissions and particles is observed for the emission at 541 nm of the type UCLNP-III. In contrast, the emission intensities of the particle types UCLNP-IV/V/VI (not depicted) show a fluctuating temperature dependency.

In addition, the possible heating effect of the infrared radiation of the NIR laser was also studied. This effect is detrimental for the measurements because the heating rate cannot be controlled and renders exact temperature determination impossible. The investigation of this effect consisted of the recording of the intensity at 541 nm for five minutes at different temperatures. **Figure 6** shows the progress of these measurements and clearly indicate that the temperature is constant over time. Therefore, an impact of the NIR laser on the sample temperature can be excluded for all studies.

3.3. Ratiometric evaluation

The intensity ratios of the peaks A/B or B/C for Er^{3+}, D/E for Ho^{3+} and F/G for Tm^{3+} were used to calculate T. Plots of the ratios of the bands A and B (I_A/I_B) and of the bands B and C (I_B/I_C) of erbium are plotted vs. T in **Figure 7**. The graphs show similar ratio values at all temperatures. The only exception is the ratio A/B of UCLNP-I which is approximately twice as high as the ratios of UCLNP-II and UCLNP-III. Furthermore, the ratio B/C increases more strongly with temperature than the ratio A/B. This is a consequence of a stronger difference between the temperature dependencies of peak B and C (with almost no

intensity change with increasing temperature) compared to the difference between peak A and B. Consequently, the ratio B/C yields a higher temperature resolution than the ratio A/B. Additionally, the deviations of the calculated ratios from the linear regression differ among the three types of UCLNPs. The ratios with the lowest variation can be observed for the particle type UCNP-III.

Figure 8 shows the intensity ratios of the peaks D and E (I_D/I_E) for holmium(III) and of the peaks F and G (I_F/I_G) for thulium(III) plotted against T. Both the range of the ratio values and the deviations from the linear regression of the holmium-doped particles are similar to those of the ratio A/B of the Er^{3+}-doped particles. However, the standard deviations of the measurements using Ho^{3+}-doped UCLNPs were much higher, and this results in a lower resolution. Thulium-doped particles display a temperature response of the ratio F/G that is only half as high as those of the other particle types, and the measurements show higher deviations from the linear regression at almost all temperatures as evidenced by a high standard deviation. As a consequence, resolution is by far lower in this case compared to other dopants.

It is important to note that ratiometric measurements have a variety of advantages in terms of precision. For example, ratiometric data are independent of variations of the intensity of the (laser) light source and drifts in the photodetector. UCLNPs with their multiple emission bands are ideally suited for ratiometric sensing. In fact, the use of probes displaying only a single emission may require the addition of a second (reference) fluorophore.

3.4. Temperature resolutions

Resolution (r_T) is an important issue when establishing calibration plots. r_T is defined as the ratio between the standard deviation (σ_T) at a specific T and the slope of the fit (S). We find that the nanoparticles with citrate as ligands (UCLNP-II and UCLNP-III) display a better resolution than those synthesized via co-precipitation (UCLNP-I). These citrate particles are better dispersible due to their smaller size and the stabilizing effects of the ligand. This results in more reproducible spectra with lower noise and, thus, in better resolutions. This phenomenon is reversed for the particle types UCLNP-IV and UCLNP-V. The resolutions that can be obtained with the various particles and the peaks used for calculating the ratios are given in **Table 2**.

The data of **Table 2** shows that the UCLNP-III enable resolutions at an average of 0.5 °C and therefore are best suited for sensing T. This is mainly due to the higher brightness of these particles and the resulting smaller standard deviation of the data points. The resolution of the two other materials (UCLNP-I and UCLNP-II) also is in the range of ±1 °C over certain intervals but on average it is 3.4 °C and 2.1 °C, respectively. These values are lower compared to the holmium- and thulium-doped particle types UCLNP-IV/V/VI.

4. Conclusion

Core-shell UCLNPs of the type $NaYF_4:Yb^{3+},Er^{3+}$ in the hexagonal phase are the optimal choice for temperature measurements in the physiologically important range between 20 – 45°C because of their brightness and the excellent temperature resolution of 0.45°C. By contrast, the temperature resolution of UCLNPs of the type $NaYF_4$ doped with other lanthanide ions (e.g. holmium and thulium) yielded lower resolutions.

UCLNPs enable a ratiometric (i.e. self-referenced and thus robust) luminescent readout in nm dimensions and with zero background due to NIR photoexcitation. Typical fields of applications include sensing temperature in synthetic nm-sized structures and machines. Other conceivable applications are temperature measurements in micro- and nanofluidic systems[39,40], in micro/nano/femto-volume (bio)chemistry[41], and synthetic chemistry[42], in thermally induced drug release[43], and wherever exothermal chemical[44] or enzymatic reactions[45] occur on a micro- or nanoscale. Thus, we believe that this method has a wide scope.

Notes and references

Institute of Analytical Chemistry, Chemo- & Biosensors, University of Regensburg, 93040 Regensburg, Germany.
E-mail: Hans-Heiner.Gorris@chemie.uni-r.de;
Otto.Wolfbeis@chemie.uni-r.de

1 S. Wang, S. Westcott, W. Chen, *J. Phys. Chem. B*, 2002, **106**, 11203-11209
2 L. R. Hirsch, R. J. Stafford, J. A. Bankson, S. R. Sershen, B. Rivera, R. E. Price, J. D. Hazle, N. J. Halas, J. L. West, *PNAS*, 2003, **100**, 13549–13554
3 Chie Gota, Kohki Okabe, Takashi Funatsu, Yoshie Harada, Seiichi Uchiyama, *J. Am. Chem. Soc.*, 2009, **131**, 2766–2767
4 E. Bentley; *Handbook of Temperature Measurement: Temperature and humidity measurement,* Vol. 1, *Springer*, Singapore, **1998**
5 H. S. Peng, S. H. Huang, O. S. Wolfbeis, *J. Nanopart. Res.*, 2010, **12**, 2729-2733
6 S. Nagl, M. I. J. Stich, M. Schaeferling, O. S. Wolfbeis, *Anal. Bioanal. Chem.*, 2009, **393**, 1199-1207
7 L.-N. Sun, J. Yu, H. Peng, J. Z. Zhang, L.-Y. Shi, O. S. Wolfbeis, *J. Phys. Chem. C*, 2010, **114**, 12642-12648
8 F. Martínez Ferreras, O. S. Wolfbeis, H. H. Gorris, *Anal. Chim. Acta*, 2012, **729**, 62-66
9 J. Yu, L. Sun, H. Peng, M. I. J. Stich, *J. Mater. Chem*., 2010, **20**, 6975–6981
10 H. H. Gorris, R. Ali, S. M. Saleh, O. S. Wolfbeis, *Adv. Mater.*, 2011, **23**, 1652-1655
11 D. N. Messias, M. V. D. Vermelho, A. S. Gouveia-Neto, J. S. Aitchison, *Rev. Sci. Instrum.*, 2002, **73**, 476-479
12 H. Berthou, C. K. Joergensen, *Optics Letters*, 1990, **15**, 1100-1102
13 L. H. Fischer, G. S. Harms, O. S. Wolfbeis, *Angew. Chem. Int. Ed.*, 2011, **50**, 4546-4551
14 H. Peng, M. I. J. Stich, J. Yu, L.-n. Sun, L. H. Fischer, O. S. Wolfbeis, *Adv. Mater.*, 2010, **22**, 716–719
15 F. Ye, C. Wu, Y. Jin, Y.-H. Chan, X. Zhang, D. T. Chiu, *J. Am. Chem. Soc.*, 2011, **133**, 8146–8149
16 S. K. Singh, K. Kumar, S.B. Rai, *Sensors and Actuators A*, 2009, **149**, 16-20
17 F. Wang, X. Liu, *Chem. Soc. Rev.*, 2009, **38**, 976-989
18 M. Haase, H. Schaefer, *Angew. Chem. Int. Ed.*, 2011, **50**, 5808 – 5829
19 M. Nyk, R. Kumar, T. Y. Ohulchanskyy, E. J. Bergey, P. N. Prasad, *Nano Lett.*, 2008, **8**, 3834-3838
20 F. Wang, D. K. Chatterjee, Z. Li, Y. Zhang, X. Fan, M. Wang, *Nanotechnology.*, 2006, **17**, 5786-5791
21 S. Heer, K. Koempe, H.-U. Guedel, M. Haase, *Adv. Mater.*, 2004, **16**, 2102-2105

22 R. A. Jalil, Y. Zhang, *Biomaterials*, 2008, **29**, 4122-4128
23 X. Wang, X. Kong, Y. Yu, Y. Sun, H. Zhang, *J. Phys. Chem. C*, 2007, **111**, 15119-15124
24 M. A. R. C. Alencar, G. S. Maciel, C. B. de Araújo, A. Patra, *Appl. Phys. Lett.*, 2004, **84**, 4753-4755
25 F. Wang, J. Wang, X. Liu, *Angew. Chem.*, 2010, **122**, 7618 –7622
26 J. C. Boyer, F. C. J. M. van Veggel, *Nanoscale*, 2010, **2**, 1417–1419
27 G.-S. Yi, G.-M. Chow, *Chem. Mater.*, 2007, **19**, 341-343
28 B. Dong, Z. Q. Feng, J. F. Zu, L. Bai, *J. Sol-Gel Sci. Technol.*, 2008, **48**, 303-307
29 B. Dong, D. P. Liu, X. J. Wang, T. Yang, S. M. Miao, C. R. Li, *Appl. Phys. Lett.*, 2007, **90**, 181117_1-181117_3
30 B. Dong, B. Cao, Y. He, Z. Liu, Z. Li, Z. Feng, *Adv. Mater.*, 2012, **24**, 1987–1993
31 F. Vetrone, R. Naccache, A. Zamarrón, A. J. de la Fuente, F. Sanz-Rodríguez, L. M. Maestro, E. M. Rodriguez, D. Jaque, J. G. Solé, J. A. Capobianco, *ACS Nano*, 2010, **4**, 3254-3258
32 G. Yi, H. Lu, S. Zhao, Y. Ge, W. Yang, D. Chen, L.-H. Guo, *Nano Lett.*, 2004, **4**, 2191-2196
33 Z. Li, Y. Zhang, *Nanotechnology*, 2008, **19**, 345606-345610
34 M. Lattuada, T. A. Hatton, *Langmuir*, 2007, **23**, 2158-2168
35 H. Guo, Z. Li, H. Qian, Y. Hu, I. N. Muhammad, *Nanotechnology*, 2010, **21**, 125602-125607
36 L. Feng, J. Wang, Q. Tang, L. Liang, H. Liang, Q. Su, *J. Lumin.*, 2007, **124**, 187-194
37 A. Patra, S. Saha, M. A. R. C. Alencar, N. Rakov, G. S. Maciel, *Chemical Physics Letters*, 2005, **407**, 477-481
38 A. Yin, Y. Zhang, L. Sun, C. Yan, *Nanoscale*, 2010, **2**, 953–959
39 D. Ross, M. Gaitan, L. E. Locascio, *Anal. Chem.*, 2001, **73**, 4117-4123
40 T. Robinson, Y. Schaerli, R. Wootton, F. Hollfelder, C. Dunsby, G. Baldwin, M. Neil, P. French, A. DeMello*, Lab Chip*, 2009, **9**, 3437-3441
41 H. H. Gorris, D. R. Walt, *Angew. Chem. Int. Ed,.* 2010, **49**, 3880-3895
42 A. Huebner, S. Sharma, M. Srisa-Art, F. Hollfelder, J. B. Edel, A. J. deMello, *Lab Chip*, 2008, **8**, 1244-1254
43 S.-W. Choi, Y. Zhang, Y. Xia, *Angew. Chem. Int. Ed.*, **2010**, **49**, 7904-7908
44 A. J. deMello, *Nature*, 2006, **442**, 394-402
45 A. Huebner, L. F. Olguin, D. Bratton, G. Whyte, W. T. S. Huck, A. J. deMello, J. B. Edel, C. Abell, F. Hollfelder, *Anal. Chem.*, 2008, **80**, 3890-3896

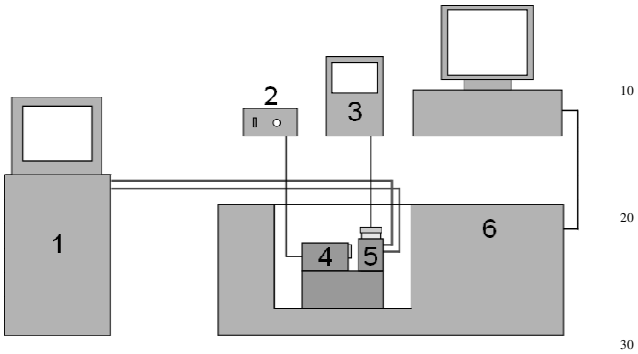

Figure 1. Experimental setup (1 thermostat, 2 laser diode, 3 resistance thermometer, 4 optical fiber waveguides, 5 cuvette, 6 fluorometer)

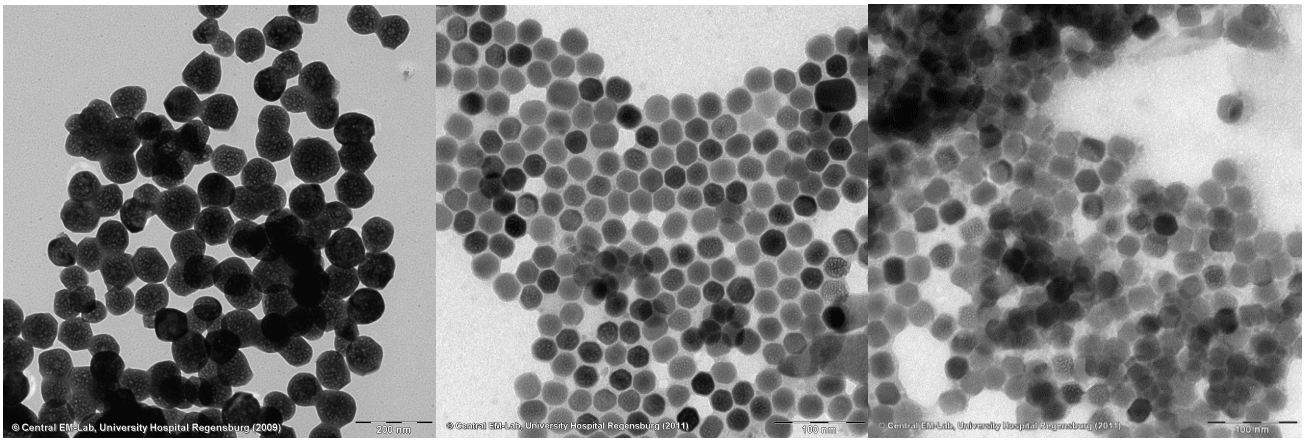

Figure 2. TEM images of different particle types (**a**: UCLNP-I with an average size of 95 – 110 nm; **b**: UCLNP-II with an average size of 25 – 30 nm, mainly hexagonal particles; **c**: UCLNP-III with an average size of 30 – 34 nm)

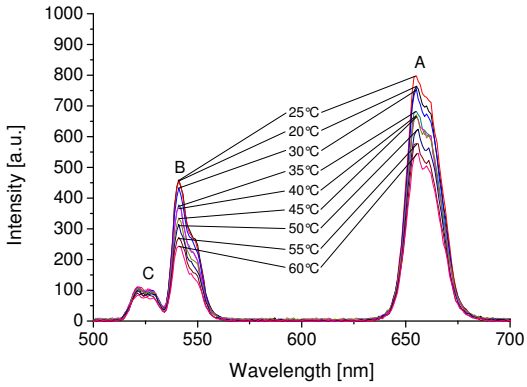

Figure 3. Emission spectra of nanoparticles of type UCLNP-I at various temperatures in water (peak A: 656 nm, peak B: 541 nm, peak C: 523 nm).

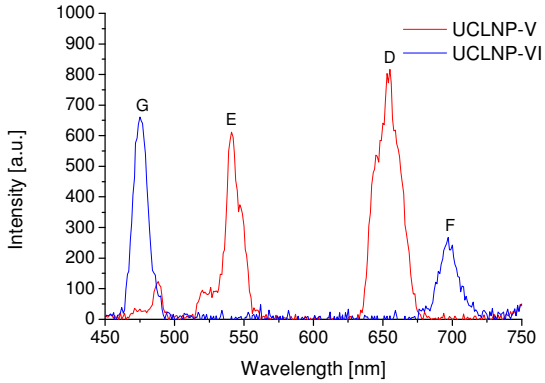

Figure 4. Emission spectra of nanoparticles of type UCLNP-V (Ho^{3+}) and UCLNP-VI (Tm^{3+}) in water (peak D: 656 nm, peak E: 541 nm, peak F: 695 nm, peak G: 475 nm).

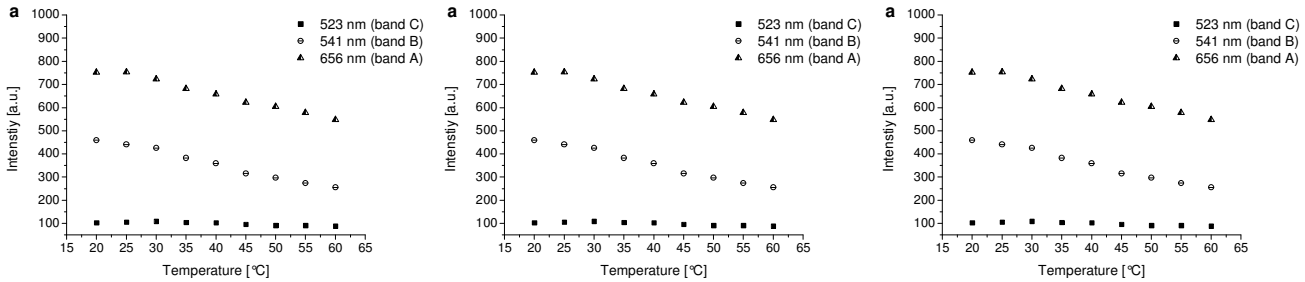

Figure 5. Intensity plots of the emissions at 523 nm, 541 nm and 656 nm for particles of the type UCLNP-I (a), UCLNP-II (b) and UCLNP-III (c).

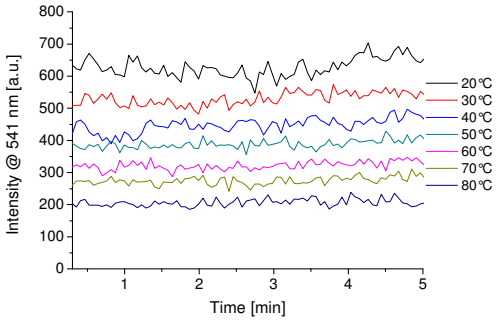

Figure 6. Intensity plots of the emissions at 541 nm over 5 minutes under NIR excitation.

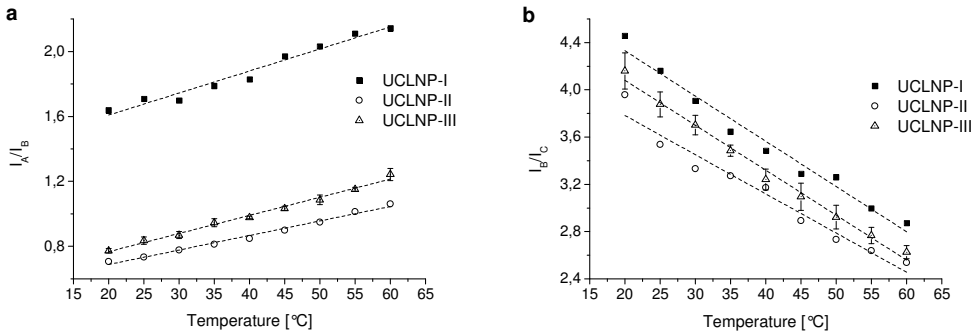

Figure 7. Ratiometric calibration plots with the respective linear fits for three types of erbium doped UCLNPs (a: I_A/I_B, b: I_B/I_C)

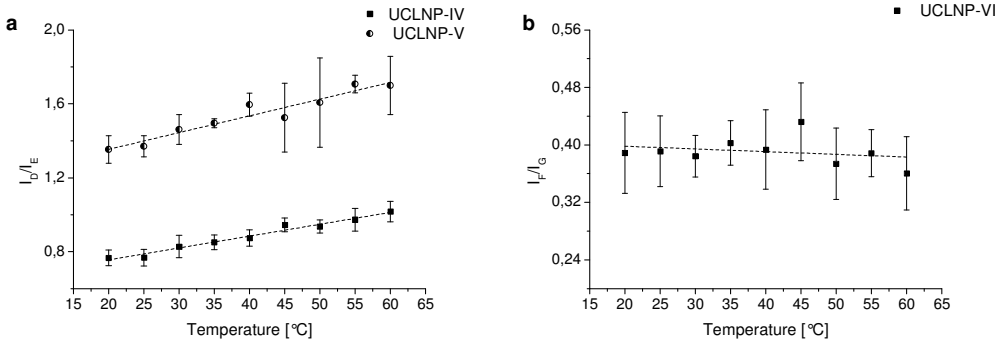

Figure 8. Ratiometric calibration plots with the respective linear fits for the holmium- (a) or thulium-doped (b) upconverting nanoparticles**.**

Table 1. Figures of merit for the particles investigated

	UCLNP-I	UCLNP-II	UCLNP-III	UCLNP-IV	UCLNP-V	UCLNP-VI
Type	$NaYF_4$:Yb, Er	$NaYF_4$:Yb, Er	$NaYF_4$:Yb, Er @ $NaYF_4$	$NaYF_4$:Yb, Ho	$NaYF_4$:Yb, Ho	$NaYF_4$:Yb, Tm
Molar percentage of dopant[a] [%]	Yb^{3+} 20, Er^{3+} 2	Yb^{3+} 20, Er^{3+} 2	Yb^{3+} 20, Er^{3+} 2	Yb^{3+} 20, Ho^{3+} 0.5	Yb^{3+} 20, Ho^{3+} 0.5	Yb^{3+} 20, Tm^{3+} 0.5
Synthesis via	co-precipitation	thermal decomposition	thermal decomposition	co-precipitation	thermal decomposition	thermal decomposition
Crystal type	mixture of cubic and hexagonal	hexagonal	hexagonal	mixture of cubic and hexagonal	hexagonal	hexagonal
Size [nm]	95 – 110	26 - 30	31 - 34	95 – 110	26 - 30	26 - 30
Surface ligand	EDTA	citric acid	citric acid	EDTA	citric acid	citric acid

[a] Referred to the total amount of rare earth ions

Table 2. Resolutions (expressed as σ_T/S) that can be obtained when sensing temperature with upconverting luminescent nanoparticles

	UCLNP-I	**UCLNP-II**	**UCLNP-III**	**UCLNP-IV**	**UCLNP-V**	**UCLNP-VI**
Ratio of bands [a]	B/C	A/B	B/C	D/E	D/E	F/G
Averaged resolution [°C]	3.4	2.1	0.45 [b] / 0.69 [c]	7.3	11.4	> 20.0

[a] see Figure 2 and 3 [b] temperature range: 20 – 45 °C [c] temperature range: 50 – 60 °C